Research Article

Visible Light-Active CdS/TiO$_2$ Hybrid Nanoparticles Immobilized on Polyacrylonitrile Membranes for the Photodegradation of Dyes in Water

Pardon Nyamukamba [ID], **Makwena Justice Moloto** [ID]**, and Henry Mungondori** [ID]

Department of Chemistry, Vaal University of Technology, Private Bag X021, Vanderbijlpark 1900, South Africa

Correspondence should be addressed to Makwena Justice Moloto; makwenam@vut.ac.za

Reusable photocatalytic polyacrylonitrile membrane-supported cadmium sulphide/titanium dioxide hybrid nanoparticles (CdS/TiO$_2$-PAN) were prepared using a dry-wet phase inversion technique. Scanning electron microscopy (SEM) analysis revealed that the photocatalytic membranes had a porous sublayer, a compact top layer, and that, some of the nanoparticles were not encapsulated by the membranes. The average crystallite sizes of the CdS, TiO$_2$, and CdS/TiO$_2$ hybrid nanoparticles were 3.41 nm, 10.47 nm, and 12.17 nm, respectively. The combination of CdS and TiO$_2$ nanoparticles led to a red shift (band gap; ca. 2.6 eV) of the absorption band and extended the optical absorption spectrum into the visible region relative to TiO$_2$. The photocatalytic activity of CdS/TiO$_2$-PAN membranes was explored in the degradation of methylene blue dye under visible light irradiation, and the results revealed that the best photocatalytic performance was achieved by 0.1 g CdS/TiO$_2$-PAN photocatalytic membrane with 5% loading of the CdS/TiO$_2$ hybrid nanoparticles, which degraded 66.29% of methylene blue in 210 minutes at 25°C and pH 8.5. It was found that the optimum loading of nanoparticles in the membranes was 0.1 g. All the photocatalytic membranes showed an insignificant decrease in the photocatalytic activity when used repeatedly. According to literature, CdS/TiO$_2$-PAN photocatalytic membranes have not been prepared before for the purpose of treating simulated wastewater.

1. Introduction

Clean water is essential to life as it is a fundamental human need. A lot of people are dying due to water-related diseases, which means that safe drinking water is of great importance. Conventional methods of water treatment are either ineffective and/or expensive; hence, there is a clear need for the improvement and development of new techniques for water treatment. Photocatalysis is one of the promising methods widely used to solve environmental pollution problems, particularly in the removal of organic contaminants due to easy operation and ability to completely photodegrade the organics into harmless products such as carbon dioxide and water.

There are several semiconductor photocatalysts that can be used in photocatalysis; however, titanium dioxide (TiO$_2$) is considered to be one of the most suitable photocatalyst due to its attracting properties such as photostability and relative nontoxicity [1]. The major drawback of TiO$_2$ is its wide band gap (3.2 eV) implying that it is active only under UV light which is <5% of the total solar radiation [2, 3]. A lot of efforts using different approaches such as sensitization [2], codoping [4], and nonmetal doping [5] have been put to make TiO$_2$ active in the visible region which constitutes about 55% of the solar radiation. Contrarily, cadmium sulphide (CdS) is absorbed in the visible region and is considered as a potential photocatalyst, but it exhibits poor quantum efficiency due to its instability in solution and results in the leaching of Cd^{2+} ions which are toxic [6]. Due to its narrow direct band gap of 2.4 eV, it has attracted considerable interest in photocatalysis and a lot of efforts have been made to enhance its photocatalytic stability [7]. Since no semiconductor photocatalyst is ideal, the development of an

effective photocatalyst that is both photostable and visible light active is of great significance.

In this study, CdS/TiO$_2$ hybrid nanoparticles on PAN membranes were prepared in which the CdS acts both as a photocatalyst and visible light absorber to sensitize TiO$_2$, whereas TiO$_2$ acts both as a barrier to reduce Cd^{2+} ions leaching and as cocatalyst to provide sites for the photodegradation of organic pollutants. The combination of CdS with other materials such as ZnO and TiO$_2$ has been found to improve photoefficiency and photostability and maximise interfacial areas between the two compounds resulting in enhanced catalytic properties [8]. The properties of the hybrid nanomaterials are a combination of the properties of both materials making up the hybrid system. This is advantageous as the system can compensate for the disadvantages of the individual components, and there will be synergistic effects such as improved photostability and efficient charge separation [9]. The immobilization of the photocatalyst on PAN membranes means no filtration step is required which could add extra cost to remove and recycle the photocatalyst after use. Moreover, the organic polymers have been found to stabilize the nanocrystals [10]. Momeni and coworkers prepared Ag$_2$S/NTs nanocomposites with good stability which were easy to be recycled, thus avoiding the filtration step process required for photocatalyst particles [11].

Hybrid materials are important and have been prepared for different applications. Liao et al. prepared hydrophilic hollow nanocube-functionalized thin film nanocomposite membrane for nanofiltration [12], Mungondori et al. prepared photocatalytic copolymer-grafted asymmetric membranes for degradation of bentazon in water [5], Venditti et al. developed nanocomposite membranes with possible applications in fuel cells [13], and Kadhom et al. prepared nanocomposite membranes filled with metal-organic frameworks for water desalination [14].

2. Methodology

2.1. Materials. The materials used were polyvinylpyrrolidone (PVP), hexane, 1-pentanol, cadmium chloride, potassium hydroxide, titanium tetrachloride, polyacrylonitrile (PAN, $M_w = 150\ 000$), dimethylformamide (DMF), and sodium sulphide. All chemicals were of analytical grade and were used as received.

2.2. Preparation of CdS/TiO$_2$ Hybrid Nanoparticles. PVP (1.02 g) was dissolved in a mixture of hexane (72 mL) and 1-pentanol (18 mL) in a conical flask. The contents were divided into two equal volumes and put in separate conical flasks. To one of the conical flasks, about 1.9 mL of 0.012 M cadmium chloride was added and stirred for 5 minutes. In another conical flask, about 1.9 mL of 0.012 M sodium sulphide was added and stirred for 5 minutes. The cadmium chloride solution was heated until a temperature of 85°C was attained followed by addition of sodium sulphide solution dropwise with magnetic stirring. The pH was maintained at 8 using potassium hydroxide solution. The solution was then

refluxed for two hours at 85°C. Titanium tetrachloride solution (6 mL, 9 M) was added dropwise to the contents with magnetic stirring at 400 rpm, and the resulting nanoparticles were separated by centrifugation, washed with methanol, and calcined at 300°C for two hours.

2.3. Preparation of CdS Nanoparticles. The same procedure that was used to prepare CdS nanoparticles was used to prepare cadmium sulphide nanoparticles, but without the addition of titanium tetrachloride.

2.4. Preparation of TiO$_2$ Nanoparticles. About 5 mL of titanium tetrachloride was added to 95 mL of distilled water with vigorous stirring. The solution was heated at 90°C for 20 minutes and cooled to room temperature. The pH was adjusted to 8 using potassium hydroxide and then heated for another 20 minutes. After cooling, the nanoparticles were separated from solution by centrifugation, washed with distilled water, and calcined at 300°C for two hours.

2.5. Preparation of PAN Membrane-Supported CdS/TiO$_2$ Hybrid Nanoparticles. A modified version of the method by Mungondori and coworkers [5] was used to prepare the membranes. About 0.1 g of CdS/TiO$_2$ hybrid nanoparticles and 2 g of PAN were dissolved in 18.98 mL of DMF. The solution was stirred for 2 hours to make sure that all the PAN dissolved and that the nanoparticles were well dispersed to form a homogenous solution. The procedure was repeated using different masses (0.05 and 0.2 g) of the CdS/TiO$_2$ hybrid nanoparticles. The polymer solutions (6 mL) were cast uniformly on glass plates and immersed in distilled water for the polymer to solidify at room temperature.

2.6. Photocatalytic Activity Evaluation. The photocatalytic activities of the TiO$_2$/PAN, CdS/PAN, and CdS/TiO$_2$-PAN membranes were evaluated using methylene blue at a temperature of 25°C and at pH 8.5. In a typical experiment, the 4.5 cm × 5.5 cm photocatalytic membranes were immersed in 150 mL of 10 ppm methylene blue in a flask, wrapped with aluminium foil, and magnetically stirred in the dark for 30 minutes for adsorption and desorption equilibrium to take place. The system was then irradiated with visible light (36 W). To detect the changes in methylene blue concentration with irradiation time, aliquots were taken at 30-minute intervals and analysed by a UV-Vis spectrometer at a wavelength of 665 nm. To investigate the stability of the catalysts, the recycling tests of the photocatalytic membranes were conducted three times.

2.7. Characterization. Thermogravimetric analysis (TGA) was performed on a PerkinElmer Pyris 6 manager TGA at a heating rate of 30°C/min using alumina pan as a reference from 30°C to 800°C under nitrogen atmosphere. The gas was

purged for 10 minutes before heating, and the flow rate of the nitrogen gas was 60 ml/min. Fourier transform infrared analysis was recorded on a FT-IR PerkinElmer 400 spectrometer from $4000 \, cm^{-1}$ to $400 \, cm^{-1}$ to identify the functional groups. X-ray diffraction (XRD) measurements were done using a Bruker AXS D8 advance diffractometer with Cu Ka radiation ($k = 1.5406 \, \text{Å}$) operated at 40 kV and 30 mA. Emission spectra were recorded on a PerkinElmer LS 45 PL spectrometer. Absorption spectra were measured using a PerkinElmer Lambda 20 UV-Vis spectrophotometer. The surface morphologies of the membranes were acquired using a Jeol JSM-6390 LV scanning electron microscope (USA) operated at 15 kV.

3. Results and Discussion

3.1. FTIR Spectral Analysis. The FTIR analysis was performed to identify the functional groups in titanium dioxide, cadmium sulphide, and CdS/TiO_2 hybrid nanoparticles as well as to study the interaction of the capping molecules with the surface of nanoparticles. In the spectrum of TiO_2, the broad peak in the range 900–$400 \, cm^{-1}$ was attributed to the stretching vibration of the Ti-O-Ti and Ti-O bonds as shown in Figure 1. The peak around $3445 \, cm^{-1}$ is attributed to the stretching vibration of O-H groups of adsorbed water [15]. Readsorption of water could have occurred from the ambient atmosphere since the spectra were not obtained in situ. In the spectrum of CdS, the band at $650 \, cm^{-1}$ corresponds to the Cd-S stretching band [16]. The bands at $1640 \, cm^{-1}$ and $3445 \, cm^{-1}$ are attributed to the bending vibration of water and O-H stretching of adsorbed water on the surface of CdS, respectively. In the spectrum of CdS/TiO_2, the peak due to Cd-S was not seen probably due to overlapping with Ti-O-Ti and Ti-O peaks [17]. The shift of the C=O stretching peak from $1644 \, cm^{-1}$ in the spectra of PVP to $1637 \, cm^{-1}$ in the spectra of capped CdS nanoparticles could indicate a strong interaction between the nanoparticles and the PVP. Some researchers proposed that the blue shift of the C=O group can be attributed to the change of p-π conjugation associated with the amide group of PVP arising from dissociation of PVP chains due to the presence of other species [18].

The FTIR analysis was also performed on the membranes to determine if there was any interaction between the nanoparticles and the PAN polymer. The FTIR spectra of PAN, TiO_2-PAN, CdS-PAN, and CdS/TiO_2-PAN membranes are shown in Figure 2. Besides PAN, all the three samples exhibit a broad peak between 3450 and $3400 \, cm^{-1}$ due to the adsorbed water or O—H stretching vibration of hydroxyl groups. This peak is more pronounced in the spectrum of TiO_2-PAN membrane, implying that the nanoparticles promoted the adsorption of water. The peaks at about $2936 \, cm^{-1}$ and $1450 \, cm^{-1}$ are assigned to the stretching vibration and bending vibration of methylene (-CH_2) group, respectively. The band at $2245 \, cm^{-1}$ is attributed to the nitrile (-CN) stretching mode. The peak at $1737 \, cm^{-1}$ might be due to the vibration of C=O bonds in hydrolysed PAN or residual DMF. When compared to the
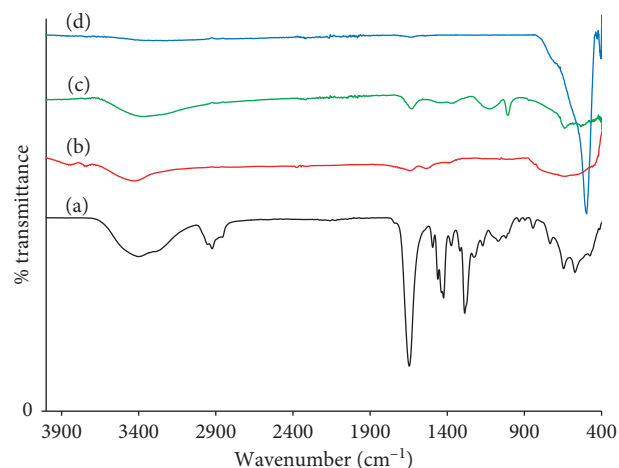

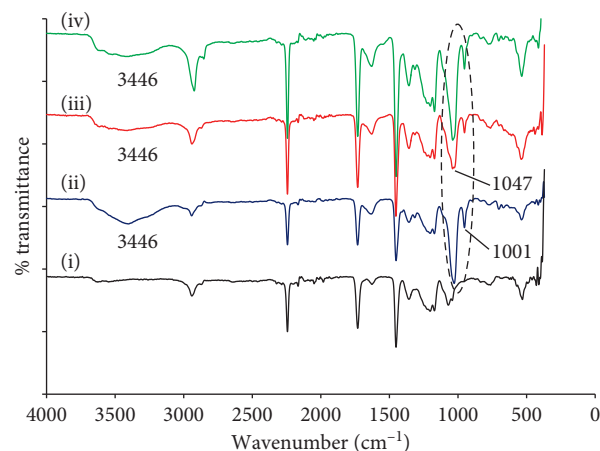Figure 1: FTIR spectra of (a) PVP, (b) TiO_2, (c) CdS, and (d) CdS/TiO_2 hybrid nanoparticles.

Figure 2: FTIR spectra of (i) PAN, (ii) TiO_2-PAN, (iii) CdS/TiO_2-PAN, and (iv) CdS-PAN membranes.

spectra of PAN, another new peak appeared around $1001 \, cm^{-1}$ in the spectrum of TiO_2-PAN, CdS-PAN, and CdS/TiO_2-PAN membranes as a result of the addition of the nanoparticles. This suggests that there may be some interactions between the nanoparticles and the polymer. There was a shift of the peak from $1086 \, cm^{-1}$ in the spectrum of PAN to $1047 \, cm^{-1}$ in the spectrum of the other three samples. Furthermore, a shift of the –C≡N vibration was not detected in the photocatalytic membranes which indicated that there was no bond formation between the –C≡N group and nanoparticles.

3.2. Optical Properties. The UV-visible absorption spectra of PVP-capped CdS, TiO_2, and CdS/TiO_2 hybrid nanoparticles are shown in Figure 3. The absorption spectra of capped CdS nanoparticles showed a characteristic absorption band with a maximum located around 500 nm as shown in Figure 3(a) (A). The absorbance band appears at shorter wavelengths in semiconductor nanocrystals when compared to the bulk (515 nm/2.4 eV) CdS material [19]. The considerable blue
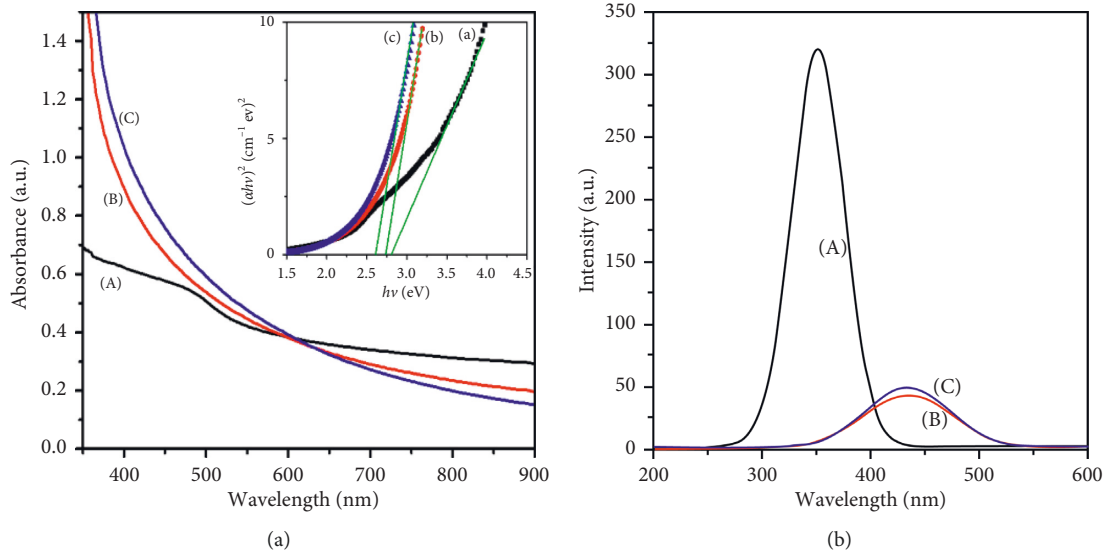
FIGURE 3: UV-Vis absorption spectra and their Tauc plots (inset) (a) and photoluminescence (PL) (b) of (A) CdS, (B) TiO$_2$, and (C) CdS/TiO$_2$ hybrid nanoparticles, respectively.

shift relative to the bulk material indicates that the CdS capped particles were formed in the quantum confinement size regime. The TiO$_2$ and CdS/TiO$_2$ hybrid nanoparticles (Figure 3(a) (B and C)) showed a band edge with $Eg = 2.73$ eV and $Eg = 2.6$ eV, respectively. The Eg was determined by plotting $(\alpha hm)^2$ versus $h\nu$ (equation (1)) and extrapolating the linear portion which intersects the energy axis $h\nu$ (inset in Figure 3(a)). The exponent n can take the value 1/2 or 2, for indirect and direct optical transition, respectively:

$$(\alpha h\nu)^2 = A (h\nu - Eg). \tag{1}$$

Combining the CdS and TiO$_2$ nanoparticles (Figure 3(a) (C)) led to a red shift of the absorption band in the hybrid nanoparticles and extends the optical absorption spectrum into the visible region when compared to that of TiO$_2$.

The fluorescence spectra of the capped CdS, TiO$_2$, and CdS-TiO$_2$ hybrid samples are shown in Figure 3(b). Figure 3(b) (A) shows the emission peak of capped CdS nanoparticles with a maximum at 352 nm. The spectral nature suggests that the particles have narrow size distribution and are monodispersed. Figure 3(b) (B and C) shows the emission peaks of TiO$_2$ and CdS/TiO$_2$ hybrid nanoparticles, respectively. The spectra show emission peaks at around 435 nm for both samples. The feature of the fluorescence band and the position of the emission maxima suggest that the fluorescence spectra exhibit band-edge emission. Band-edge emission originates from the recombination of free excitons of nanocrystalline-size regime. Usually, two emissions are observed from semiconductor nanoparticles: an excitonic and a trapped emission. The excitonic emission is usually sharp and located near absorption edge of the particles, while the trapped emission is broad and Stokes shifted [20]. The TiO$_2$ nanoparticles were more polydispersed as compared to CdS and CdS-TiO$_2$ hybrid. PL is an effective technique to

investigate the efficiency of the charge carrier trapping, migration, and transfer due to the PL signals of semiconductor materials, due to the recombination of photoinduced charge carriers. Generally, low PL intensity indicates a low recombination rate of photoinduced electron-hole pairs [21]. As shown in Figure 3, the PL intensity of pure CdS is much higher than that of the CdS/TiO$_2$ hybrid nanoparticles which demonstrates that the combination of CdS and TiO$_2$ effectively inhibits the charge carrier recombination.

3.3. XRD Analysis.
The XRD patterns of TiO$_2$, CdS, and CdS/TiO$_2$ hybrid nanoparticles are shown in Figure 4. In the XRD pattern of CdS, three peaks were found at 2θ values of 26.46°, 43.28°, and 51.20° corresponding to the (111), (220), and (311) planes, respectively, which can be indexed to cubical zincblende structure [22]. This is in good agreement with the JCPDS card (No: 10-454) corresponding to CdS. The XRD peaks were broad, indicating that the nanoparticles were very small in size which was a confirmation of the formation of nanosized particles. A mixture of cubic and hexagonal phases is normally observed in CdS nanoparticles due to transformation from one form to another due to their similar energy [23]. When the size of the CdS nanoparticles is less than 5 nm, they transform from hexagonal wurtzite-type structure to cubic zincblende structure and when above 5 nm, a mixture of both phases is observed [24]. In the XRD pattern of TiO$_2$ (Figure 4(a)), the peaks at 25.42°, 37.8°, 48.1°, 53.9°, 62.5°, 70.25°, 74.88°, and 82.25° correspond to (101), (004), (200), (105), (205), (205), (215), and (224) crystal faces of the anatase phase while the peaks at 26.66°, 54.12°, and 67.8 correspond to (110), (220), and (301) crystal faces of the rutile phase. In the XRD pattern of CdS/TiO$_2$ hybrid nanoparticles, there are no distinct peaks corresponding to CdS that were observed probably due to the insufficient amount of CdS in the CdS/TiO$_2$ hybrid nanoparticles to be
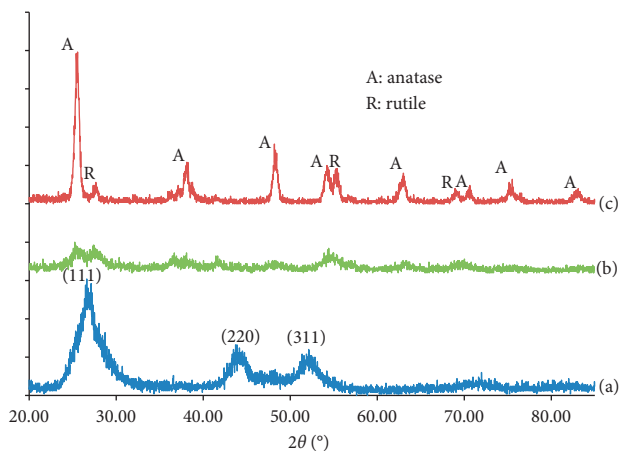
FIGURE 4: XRD patterns of (a) PVP-capped CdS, (b) CdS/TiO$_2$ hybrid, and (c) TiO$_2$ nanoparticles.

detected. The absence of distinct XRD peaks corresponding to CdS does not mean that there were no CdS nanoparticles in the hybrid as there was a considerable colour change from white of the pure TiO$_2$ to orange-yellow in the hybrid. The diameter (D) of the nanoparticles was determined by the Debye–Scherrer equation as follows:

$$D = \frac{K\lambda}{\beta \cos \theta}, \qquad (2)$$

where K is the Scherrer constant, λ is the wavelength of light used for the diffraction, β is the "full width at half maximum" of the peaks, and θ is the Bragg diffraction angle. The peaks that were used to estimate particle size were 23.46°, 43.28°, and 51.20° for CdS, 25.42°, 37.8°, and 48.1° for TiO$_2$, and 26.3°, 26.66°, and 5.9° for CdS/TiO$_2$ hybrid. The average crystallite sizes of the CdS, TiO$_2$, and hybrid CdS/TiO$_2$ nanoparticles were 3.41 nm, 10.47 nm, and 12.17 nm, respectively.

3.4. SEM Analysis of the Membranes.

The surface and the cross-sectional view of the CdS/PAN and CdS/TiO$_2$-PAN membranes are shown in Figure 5. Some surface residing nanoparticles can be seen on the surface of both membranes (Figures 5(a) and 5(b)), but they are not uniformly distributed. No visible pores were observed on the surface of the membranes. The cross-sectional view of the membranes shows that the sublayer is porous and the top layer is compact. The CdS/PAN membranes have numerous small pores when compared to the CdS/TiO$_2$-PAN membranes which have few large pores.

The EDX graphs of CdS-TiO$_2$/PAN and CdS/PAN membranes are shown in Figures 5(e) and 5(f), respectively, and they revealed the presence of carbon, titanium, nitrogen, and oxygen as expected. The peaks due to gold were also found in the spectra since all the samples were coated with gold prior to SEM analysis.

3.5. Thermal Analysis.

TGA enables the determination of the amount of moisture and volatile compounds present in the membranes, weight loss, and thermal breakdown. Figure 6 shows the thermograms of PAN, CdS-TiO$_2$/PAN, and CdS/PAN membranes. The first decomposition observed in the thermograms of CdS-TiO$_2$/PAN and CdS/PAN membranes between 30 and 156°C with a percentage weight loss of 12.34% is attributed to the loss of adsorbed water and solvent. The first percentage weight loss in the thermogram of pure PAN membrane was different from that of the other samples as it showed a continuous big weight loss of 30.54% between 30 and 150°C which is also attributed to evaporation and desorption of solvent molecules and adsorbed water (humidity). In the temperature range 150 to 280°C, the weight loss is due to dehydrogenation reactions and release of gases, such as carbon dioxide [25]. The weight loss from 280°C of all samples can be attributed to the release of gases, such as hydrogen, N$_2$, CO, CO$_2$, CH$_4$, NH$_3$, and HCN at greater intensity owing to cyclization and cross-linking of the nitrile groups of PAN [26]. In the same temperature range, the weight loss of the composites was less when compared to pure PAN, suggesting that the addition of nanoparticles stabilizes and/or delay the cyclization process which means that there could be intermolecular interaction between PAN and the nanoparticles.

3.6. Photocatalytic Activity Evaluation.

The photocatalytic activity of CdS, TiO$_2$, and CdS/TiO$_2$ hybrid nanoparticles immobilized on PAN membranes was evaluated using methylene blue under visible light. The effect of the catalyst loading was also evaluated by using membranes loaded with different amounts of CdS/TiO$_2$ hybrid nanoparticles. There was an increase in the photocatalytic activity of the membranes from 20.33% to 66.29% when the amount of CdS/TiO$_2$ hybrid catalyst was increased from 1 to 5% (w/w) (Figure 7). A further increase of the catalyst loading from 5% to 10% decreased the photodegradation probably due to a decrease in surface area owing to agglomeration of the nanoparticles. When the photocatalytic activity of CdS/TiO$_2$ hybrid catalyst is compared to that of pure CdS of the same loading, it was observed that the hybrid had a higher photocatalytic activity. This is probably attributed to the synergistic effect between the CdS and TiO$_2$ nanoparticles and better charge transfer between CdS and TiO$_2$. Similar results were obtained where sensitised TiO$_2$ showed enhanced photocatalytic performance due to synergistic effects [27]. Since the TiO$_2$ nanoparticles cannot absorb visible light, the observed photodegradation process should have been initiated by CdS nanoparticles which are visible light sensitive. The possible mechanism for the photodegradation of methylene blue involves electron transfer from the conduction band of excited CdS to the conduction band of TiO$_2$ as shown in Figure 7.

The flow of electrons from CdS nanoparticles to TiO$_2$ nanoparticles is possible due to the fact that the conduction band of CdS (−0.8 V vs. NHE) is −0.5 V more negative than that of TiO$_2$ (−0.3 V vs. NHE) [28]. The electrons may then reduce dissolved oxygen in water in contact with the photocatalyst to form highly reactive oxygen species which
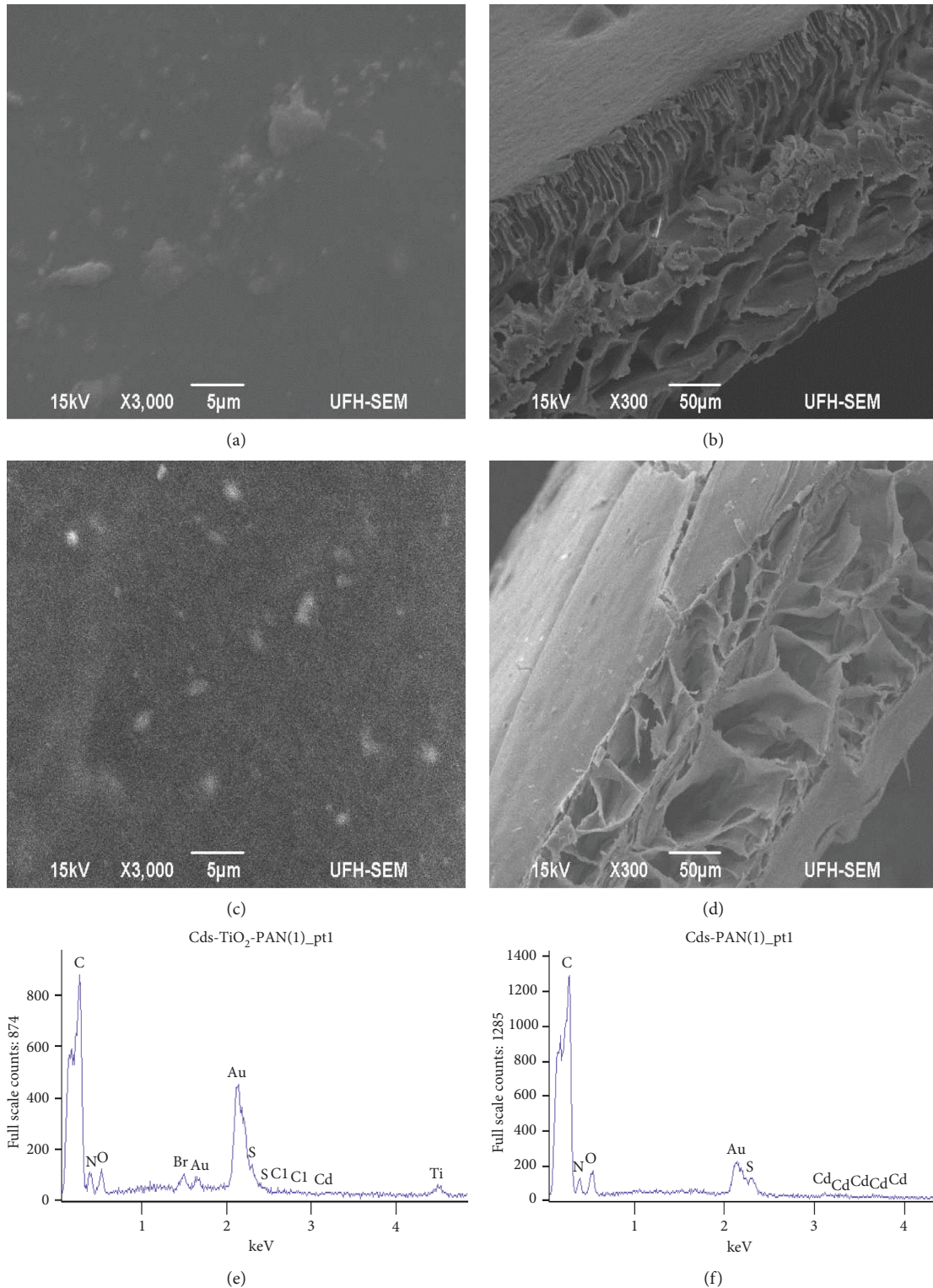
(a)

(b)

(c)

(d)

(e)

(f)

FIGURE 5: SEM images and cross-sectional view of (a, b) CdS/PAN membranes and (c, d) CdS/TiO$_2$-PAN membranes and EDX graphs of (e) CdS/TiO$_2$-PAN and (f) CdS/PAN membranes.

then oxidize methylene blue. However, since the valence band of CdS is smaller than the valence band of TiO$_2$, the holes cannot be transferred to the valence band of TiO$_2$ resulting in the inhibition of the recombination between electrons and holes [29]. The holes can also react with water

or hydroxyl ions to form hydroxyl radicals which also degrade the methylene blue (Figure 7). The reduced electron-hole recombination in the hybrid could also explain why CdS nanoparticles were less photocatalytically active when compared to the hybrid nanoparticles of
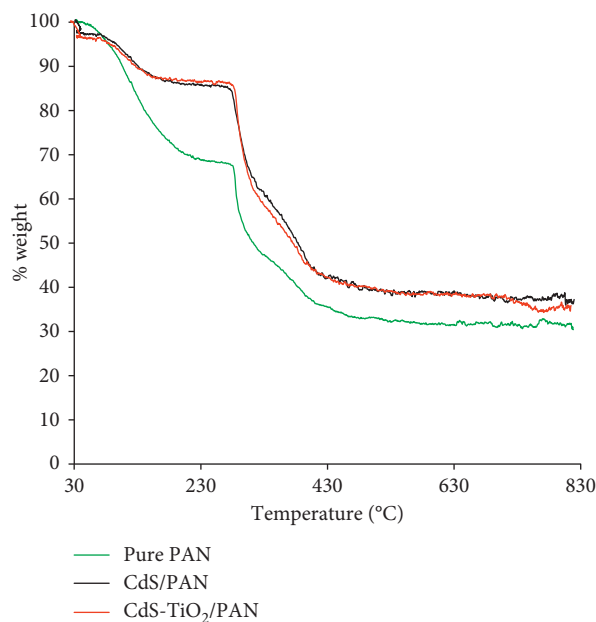
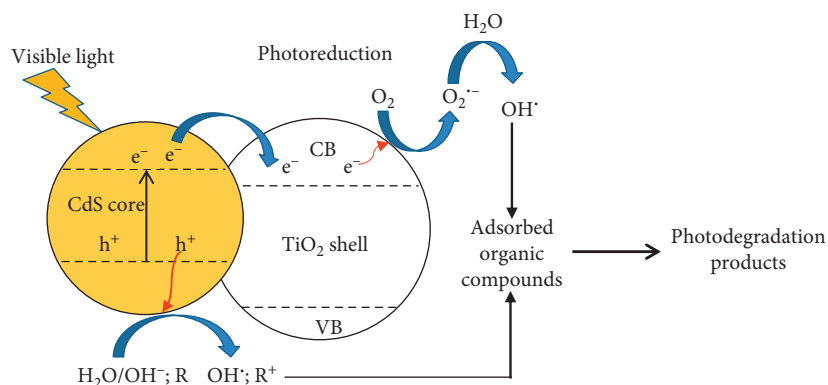FIGURE 6: TGA thermograms of pure PAN, CdS-TiO$_2$/PAN, and CdS/PAN membranes.

FIGURE 7: Proposed photoinduced electron-hole pair formation mechanism at the CdS-TiO$_2$ hybrid nanoparticle surface.

equivalent loading. TiO$_2$-PAN membranes did not show any photocatalytic activity under visible light as there was no noticeable change in the concentration of methylene blue with time.

Recycling experiments were carried out to evaluate the stability and durability of 0.2 g CdS/TiO$_2$-PAN, 0.1 g CdS/ TiO$_2$-PAN, and 0.1 g CdS-PAN by determining the change in efficiency of the photocatalysts with repeated use, and the results are shown in Figure 8. The reusability of 0.05 g CdS/ TiO$_2$-PAN was not tested since its photocatalytic activity was low in the first cycle. For the 0.2 g CdS/TiO$_2$-PAN photocatalyst, there was an insignificant loss in photocatalytic activity with repeated use. The total amount of methylene blue photodegraded decreased slightly from 55.01% in the first cycle to 51.34% in the second cycle and 47.43% in the third cycle when 0.1 g CdS-PAN photocatalyst was used. The 0.1 g CdS/TiO$_2$-PAN photocatalytic membrane photodegraded 66.71%, 66.26%, and 60.37% in the first, second, and third cycles, respectively. Generally, the overall changes

in the photocatalytic activity were low for all the photocatalysts, and since the efficiency of a photocatalyst in a given process is a significant component for determining its economic viability, their application may be economically viable. It is known that the use of powdered nanoparticles results in higher photocatalytic activity than immobilized nanoparticles. However, the nanoparticles can be easily removed from the aqueous solution due to the application of membranes.

4. Conclusion

Photocatalytic CdS/TiO$_2$-PAN membranes were successfully prepared, characterised, and tested for the photodegradation of methylene blue. The study showed that an increase in nanoparticle loading in the membranes increased the photocatalytic activity until an optimum loading of 5% and further increment had a detrimental effect. CdS/TiO$_2$-PAN membranes showed higher photocatalytic activity than CdS-
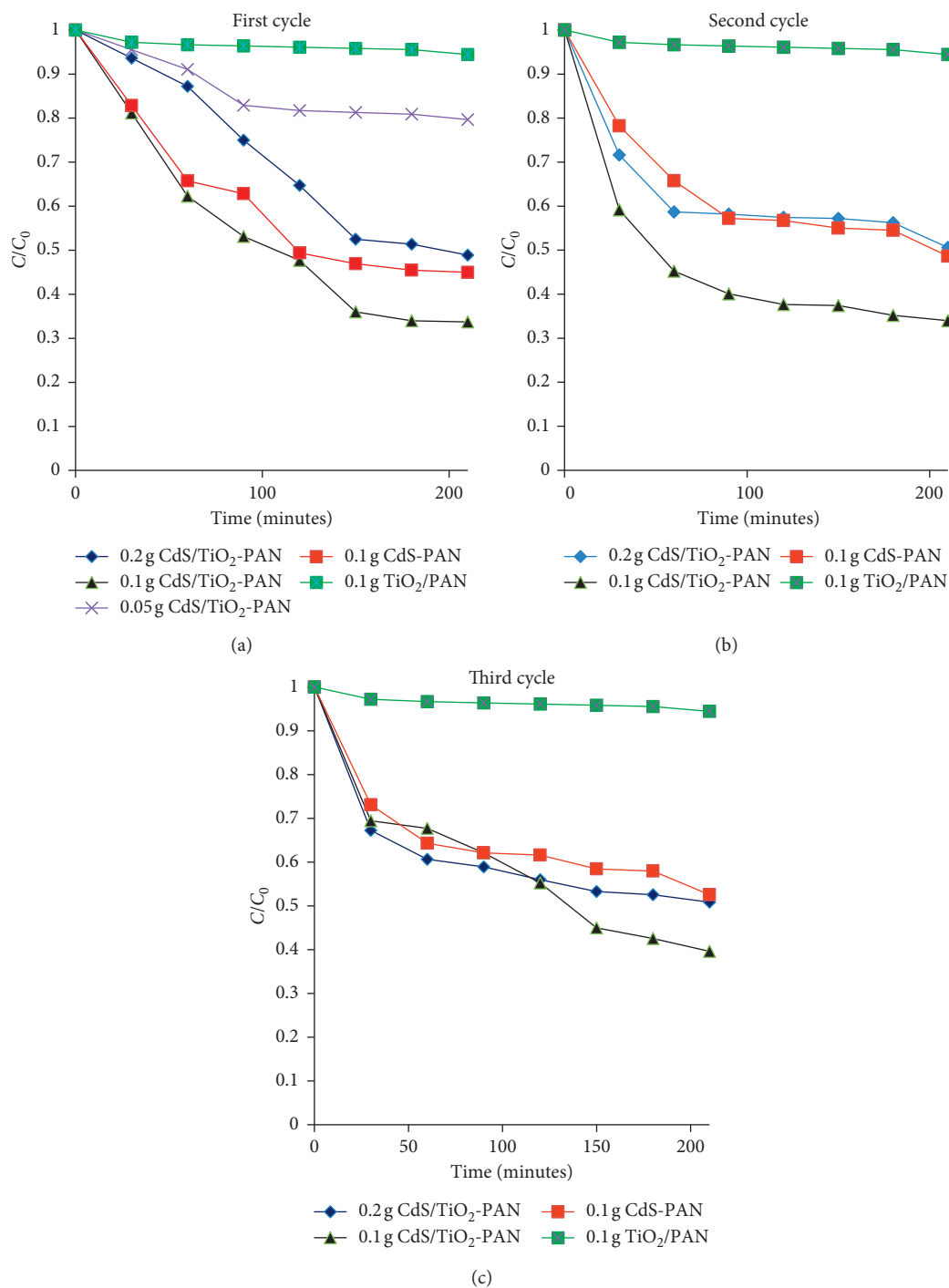
(a)

(b)

(c)

Figure 8: Photodegradation profiles of 150 mL of 10 ppm methylene blue using photocatalytic membranes with different catalyst loadings under visible light at 25°C and pH 8.5.

PAN with the same nanoparticle loading due to the suppression of the undesirable electron kinetics which includes trapping at the surface defects of the TiO_2 and reduced charge recombination. The loss in efficiency of the photocatalysts was very small with repeated use implying that there is a possibility of their application for the removal of organic contaminants in water. It could be concluded that the high photocatalytic activity of CdS/TiO_2-PAN photocatalytic membrane when compared to CdS-PAN and TiO_2-PAN was attributed to the good contact between CdS and TiO_2 and efficient separation of charge carriers.

Data Availability

The data used to support the findings of this study are included within the article.

Conflicts of Interest

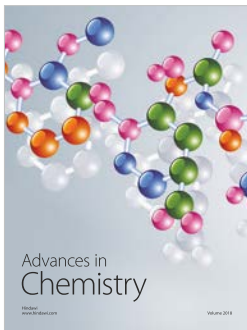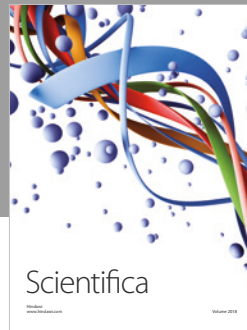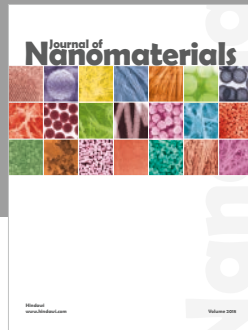The authors declare that they have no conflicts of interest.

Acknowledgments

References

[1] W.-J. Ong, L.-L. Tan, S.-P. Chai, S.-T. Yong, and A. R. Mohamed, "Facet-dependent photocatalytic properties of TiO_2-based composites for energy conversion and environmental remediation," *ChemSusChem*, vol. 7, no. 3, pp. 690–719, 2014.

[2] J. Yao, H. Chen, F. Jiang, Z. Jiao, and M. Jin, "Titanium dioxide and cadmium sulfide co-sensitized graphitic carbon nitride nanosheets composite photocatalysts with superior performance in phenol degradation under visible-light irradiation," *Journal of Colloid and Interface Science*, vol. 490, pp. 154–162, 2017.

[3] W. Dong, F. Pan, L. Xu et al., "Facile synthesis of CdS@TiO_2 core–shell nanorods with controllable shell thickness and enhanced photocatalytic activity under visible light irradiation," *Applied Surface Science*, vol. 349, pp. 279–286, 2015.

[4] P. Nyamukamba, L. Tichagwa, S. Mamphweli, and L. Petrik, "Silver/carbon codoped titanium dioxide photocatalyst for improved dye degradation under visible light," *International Journal of Photoenergy*, vol. 2017, Article ID 3079276, 9 pages, 2017.

[5] H. H. Mungondori, L. Tichagwa, D. M. Katwire, and O. Aoyi, "Preparation of photo-catalytic copolymer grafted asymmetric membranes (N-TiO_2-PMAA-g-PVDF/PAN) and their application on the degradation of bentazon in water," *Iranian Polymer Journal*, vol. 25, no. 2, pp. 135–144, 2016.

[6] N. Qutub, B. M. Pirzada, K. Umar, O. Mehraj, M. Muneer, and S. Sabir, "Synthesis, characterization and visible-light driven photocatalysis by differently structured CdS/ZnS sandwich and core-shell nanocomposites," *Physica E: Low-Dimensional Systems and Nanostructures*, vol. 74, pp. 74–86, 2015.

[7] S. A. Macías-Sánchez, R. Nava, V. Hernández-Morales et al., "$Cd_{1−x}Zn_xS$ solid solutions supported on ordered mesoporous silica (SBA-15): structural features and photocatalytic activity under visible light," *International Journal of Hydrogen Energy*, vol. 37, no. 13, pp. 9948–9958, 2012.

[8] N. Ghows and M. H. Entezari, "Exceptional catalytic efficiency in mineralization of the reactive textile azo dye (RB5) by a combination of ultrasound and core-shell nanoparticles (CdS/TiO_2)," *Journal of Hazardous Materials*, vol. 195, pp. 132–138, 2011.

[9] N. Ghows and M. H. Entezari, "Sono-synthesis of core-shell nanocrystal (CdS/TiO_2) without surfactant," *Ultrasonics Sonochemistry*, vol. 19, no. 5, pp. 1070–1078, 2012.

[10] H. Yoon, J. Lee, D. W. Park, C. K. Hong, and S. E. Shim, "Preparation and electrorheological characteristic of CdS/polystyrene composite particles," *Colloid and Polymer Science*, vol. 288, no. 6, pp. 613–619, 2010.

[11] M. M. Momeni, Y. Ghayeb, and A. A. Mozafari, "Optical and photo catalytic characteristics of Ag_2S/TiO_2 nanocomposite films prepared by electrochemical anodizing and SILAR approach," *Journal of Materials Science: Materials in Electronics*, vol. 27, no. 11, pp. 11201–11210, 2016.

[12] Z. Liao, X. Fang, J. Xie et al., "Hydrophilic hollow nanocube-functionalized thin film nanocomposite membrane with enhanced nanofiltration performance," *ACS Applied Materials & Interfaces*, vol. 11, no. 5, pp. 5344–5352, 2019.

[13] I. Venditti, L. Fontana, F. Scaramuzzo et al., "Nanocomposite based on functionalized gold nanoparticles and sulfonated poly(ether ether ketone) membranes: synthesis and characterization," *Materials*, vol. 10, no. 3, p. 258, 2017.

[14] M. Kadhom, W. Hu, and B. Deng, "Thin film nanocomposite membrane filled with metal-organic frameworks UiO-66 and MIL-125 nanoparticles for water desalination," *Membranes*, vol. 7, no. 2, p. 31, 2017.

[15] C. A. Páez, D. Poelman, J.-P. Pirard, and B. Heinrichs, "Unpredictable photocatalytic ability of H_2-reduced rutile-TiO_2 xerogel in the degradation of dye-pollutants under UV and visible light irradiation," *Applied Catalysis B: Environmental*, vol. 94, no. 3-4, pp. 263–271, 2010.

[16] S. B. Kakodkar, "Synthesis, characterisation and photocatalytic activity of cadmium sulphide nanoparticles," *Chemical Science Transactions*, vol. 5, no. 1, pp. 75–78, 2016.

[17] A. B. Lavand, Y. S. Malghe, and S. H. Singh, "Synthesis, characterization, and investigation of visible light photocatalytic activity of C doped TiO2/CdS core-shell nanocomposite," *Indian Journal of Materials Science*, vol. 2015, Article ID 690568, 9 pages, 2015.

[18] K. Sivaiah, R. B. Hemalatha, and S. Buddhudu, "Structural, thermal and optical properties of Cu^{2+} and Co^{2+}: PVP polymer films," *Indian Journal of Pure and Applied Physics*, vol. 48, pp. 658–662, 2010.

[19] R. Elilarassi, S. Maheshwari, and G. Chandrasekaran, "Structural and optical characterization of CdS nanoparticles synthesized using a simple chemical reaction route," *Optoelectronics and Advanced Materials*, vol. 4, no. 3, pp. 309–312, 2010.

[20] P. K. Khanna, R. R. Gokhale, V. V. V. S. Subbarao, N. Singh, K.-W. Jun, and B. K. Das, "Synthesis and optical properties of CdS/PVA nanocomposites," *Materials Chemistry and Physics*, vol. 94, no. 2-3, pp. 454–459, 2005.

[21] Y. Huo, J. Zhang, X. Chen, and H. Li, "Synthesis of hollow CdS-TiO_2 microspheres with enhanced visible-light photocatalytic activity," *International Journal of Photoenergy*, vol. 2012, Article ID 907290, 5 pages, 2012.

[22] S. K. Mishra, R. K. Srivastava, S. G. Prakash, R. S. Yadav, and A. C. Panday, "Structural, optical and photoconductivity characteristics of manganese doped cadmium sulfide nanoparticles synthesized by co-precipitation method," *Journal of Alloys and Compounds*, vol. 513, pp. 118–124, 2012.

[23] S. Takeuchi and K. Suzuki, "Stacking fault energies of tetrahedrally coordinated crystals," *Physica Status Solidi (a)*, vol. 171, no. 1, pp. 99–103, 1999.

[24] S. Mathew, S. Ani Joseph, P. Radhakrishnan, V. P. N. Nampoori, and C. P. G. Vallabhan, "Shifting of fluorescence peak in CdS nanoparticles by excitation wavelength change," *Journal of Fluorescence*, vol. 21, no. 4, pp. 1479–1484, 2011.

[25] A. T. Kuvarega, R. W. M. Krause, and B. B. Mamba, "Nitrogen/palladium-codoped TiO_2 for efficient visible light photocatalytic dye degradation," *Journal of Physical Chemistry C*, vol. 115, no. 45, pp. 22110–22120, 2011.

[26] G. P. Wu, C. X. Lu, L. C. Ling, and Y. G. Lu, "Comparative investigation on the thermal degradation and stabilization of carbon fiber precursors," *Polymer Bulletin*, vol. 62, no. 5, pp. 667–678, 2009.

[27] M. M. Momeni, Y. Ghayeb, and F. Ezati, "Fabrication, characterization and photoelectrochemical activity of tungsten-copper co-sensitized TiO$_2$ nanotube composite photoanodes," *Journal of Colloid and Interface Science*, vol. 514, pp. 70–82, 2018.

[28] C. Gao, Z. Wang, Z. Yu et al., "Effect of pH values on photocatalytic properties of Bi$_2$WO$_6$ synthesized by hydrothermal method," *Journal of Wuhan University of Technolotgy-Mater. Sci. Ed.*, vol. 24, no. 4, pp. 533–536, 2009.

[29] T. T. D. Vu, F. Mighri, A. Ajji, and T.-O. Do, "Synthesis of titanium dioxide/cadmium sulfide nanosphere particles for photocatalyst applications," *Industrial & Engineering Chemistry Research*, vol. 53, no. 10, pp. 3888–3897, 2014.